Electrochimica Acta 325 (2019) 134957

Contents lists available at ScienceDirect

Electrochimica Acta

journal homepage: www.elsevier.com/locate/electacta

Electrode stimulation: Redox reactions induced by modulating the electrostatic potential in solution

Qi Han [a], Nicholas S. Georgescu [a], John Gibbons [b], Daniel Scherson [a, *]

[a] Department of Chemistry, Case Western Reserve University, Cleveland, OH, 44106, United States
[b] Department of Electrical Engineering and Computer Science, Case Western Reserve University, Cleveland, OH, 44106, United States

ARTICLE INFO

Article history:
Received 27 August 2019
Received in revised form
24 September 2019
Accepted 24 September 2019
Available online 25 September 2019

Keywords:
Kinetics
Electrostatic potential
Overpotential

ABSTRACT

The rates of model heterogeneous redox reactions have been modulated by changing the electrostatic potential in the solution immediately adjacent to a working electrode, (WE), kept at a fixed value with respect to a reference electrode. The approach involves passing current between a stimulating electrode (SE) placed in front and at a short distance from the WE and a distant counter electrode. Conditions were selected so that the potential distribution in solution closely approximates that prescribed by the primary current distribution and thus maintain the electrolyte composition in the region between SE and WE virtually unperturbed. Illustrations are provided for the formation of gold oxide and the oxidation of adsorbed carbon monoxide on Pt in acidic aqueous electrolytes.

© 2019 Elsevier Ltd. All rights reserved.

1. Introduction

The rates of elementary heterogeneous electron transfer reactions at electrode|electrolyte interfaces are often expressed in terms of the Butler-Volmer equation, i.e.

$$i = i_o\{\exp(\alpha_a nF\eta_s / RT) - \exp(-\alpha_c nF\eta_s / RT)\} \quad (1)$$

In this expression, η_s, the surface overpotential, is defined as "*the potential of the working electrode, WE, E_{WE}, relative to a reference electrode, RE, of the same kind placed in the solution adjacent to the surface of the WE.*" [1], i_o is known as the exchange current density, a parameter that depends on the composition of the electrolyte next to the electrode surface, and all other terms have their common significance. To date, virtually all fundamental information regarding electrode processes has been obtained by controlling the potential of the electrode with respect to a RE placed in the bulk solution, E_{WE}, using a potentiostat [2]. Full verification of this formalism requires for the rates to be modified by changing the electrostatic potential "just outside the double layer", ϕ_{dl}, and thus η_s, while keeping E_{WE} constant. This article describes means to accomplish this goal opening new prospects for gaining a better understanding of the factors that govern these important interfacial processes.

The specific arrangement employed in our experiments involves either a Au or Pt microdisk (μ-WE), and a larger Pt disk, to be referred to hereafter as the ***stimulating*** electrode, SE, placed parallel to the μ-WE at a distance δ, with their main axes aligned along their normal centerline (see A, Fig. 1). The SE is mounted on a micrometer, allowing the distance between it and the working electrode to be accurately controlled. During the experiments, a bipotentiostat is used to fix E_{WE}, while the potential of the SE, is scanned between two judiciously selected limits. The current that flows between the SE and the counter electrode (not shown in the figure), i_{SE} (see thick arrows in Panels B and C, Fig. 1), will generate a potential drop in the electrolyte, which, depending on the sign of i_{SE}, will bring about a decrease, or an increase in ϕ_{dl} (see red and blue circles in B and C, respectively) with respect to its original value (violet circle) [3]. Under such conditions, η_s will correspondingly increase or decrease (see double arrows in B and C, in this figure) and potentially induce oxidation or reduction reactions at the WE, respectively, for which the rates can be measured by monitoring the current, i_{WE}, flowing through that electrode.

Whether such processes will be observed will depend critically on the values of E_{WE}, δ, and the sign and magnitude of i_{SE}. An illustration of electron transfer reactions induced by changes in the electrostatic potential in solution, ϕ_{el}, is provided by the emerging area of bipolar electrochemistry, whereby current flowing between two electrodes elicits a potential drop within the solution leading to changes in η_s along an electrode placed in its path ***without any external connections***. As described in numerous publications, this

* Corresponding author.
E-mail address: dxs16@case.edu (D. Scherson).

https://doi.org/10.1016/j.electacta.2019.134957
0013-4686/© 2019 Elsevier Ltd. All rights reserved.

tactic can give rise to local oxidation and reduction currents in different regions of this ***floating*** or ***bipolar electrode***, such as metal deposition and metal plating [4,5]. Particularly noteworthy is the work of Kayran et al. [6], who measured local potential differences along the length of bipolar electrodes using a scanning micro-reference electrode, to study correlations between the nature of Au nanovoids and their surface enhanced Raman activity. It should be emphasized that the fact that the current flowing through such bipolar electrodes cannot be independently measured, and the actual potential distribution in solution is seldom well-defined, makes it very difficult to establish correlations between η_s and the rates of interfacial electron transfer, which are of critical fundamental importance and constitute the major focus of the electrode stimulation technique.

The approach described in this work overcomes these limitations by allowing i_{WE} to be accurately measured under experimental conditions where ϕ_{el} is prescribed by the primary current distribution. As shown in our earlier publications in the area of ohmic microscopy [7–9], the latter can be achieved by scanning the potential of a metal disk made out of, for example Pt or Au, embedded in an insulating surface, in fully deaerated sulfuric or perchloric aqueous solutions, within a potential range in which the interface behaves as a pure capacitor or a pseudocapacitor. In this fashion, the composition of the electrolyte adjacent to the SE remains virtually unchanged during the stimulation and hence plays no role in controlling the rate of redox reactions at the WE. The term ***electrode stimulation*** appears uniquely appropriate, as the phenomenon in question bears close similarity to functional neural stimulation, whereby a negative current of appropriate magnitude is applied between an electrode close to the neural membrane and a distant electrode. This perturbation causes a local depolarization of the membrane triggering an electrical signal, or action potential, that propagates along the nerve [10]. It should be emphasized that a quantitative interpretation of electrode stimulation, as implemented in this work, is based on a theoretical analysis of primary current and potential distribution for a fourelectrode system. This specific subject received considerable attention several decades ago, as illustrated by the seminal contributions of Gabrielli et al. [11], and Miksis and Newman [12], who examined a system consisting of a disk electrode, a concentric ring electrode, i.e. the geometry of a conventional rotating ring-disk electrode, and a large counter electrode placed at infinity. Their analysis concluded that three independent resistance values describe the primary potential difference between any two electrodes. A more recent review of the literature in this area was published by Trinh et al. [13] in connection to their analysis of cross-talk between electrodes in transient scanning electrochemical microscopy, SECM, in the strict absence of redoxactive species in solution.

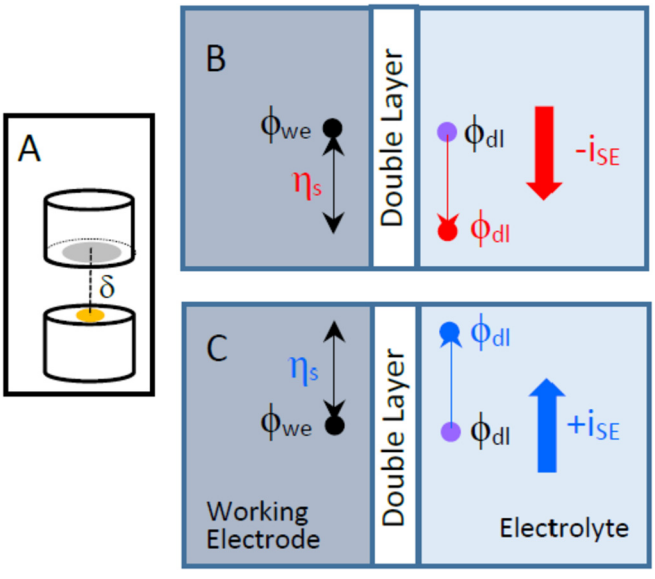

Fig. 1. Schematic diagram of A. the WE|SE arrangement used for the electrode stimulation experiments. B&C. the changes in the surface overpotential, η_s, at the WE, induced by the flow of negative ($-i_{SE}$, red, upper panel) and positive current ($+i_{SE}$, blue, lower panel) through the SE. The shifts in η_s are indicated by the double black arrows in these panels.

2. Experimental

The body of the electrochemical cell used in our experiments was a polypropylene centrifuge tube (Fisherbrand, 50 mL, STK# 0644320) with its bottom end cut off to expose a circular hole ca. 5 mm in diameter. A schematic diagram of the assembled cell is shown in Fig. 2. As indicated therein, WE was either a commercial Au microelectrode (CH Instruments, CHI 105, diameter 12.5 μm), Au(μ-WE), or a Pt(μ- WE) (Basi, MF-2150, diameter 100 μm), inserted into the hole of the cell facing upwards, and a carbon rod (Alfa Aesar, diameter 3.05 mm) and a Ag/AgCl (Basi, MF2052) were

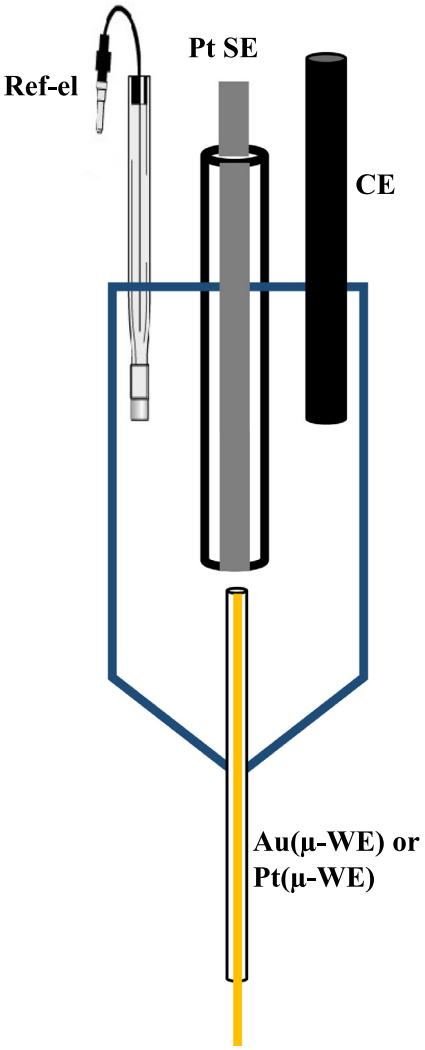

Fig. 2. Schematic diagram of the electrochemical cell used for the electrode stimulation experiments.

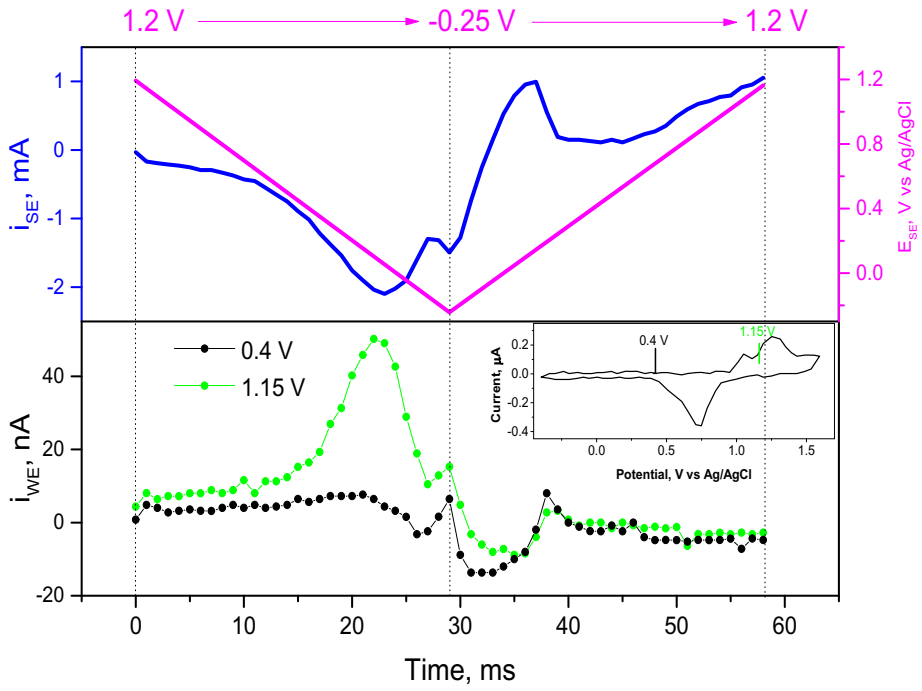

Fig. 3. Plots of i_{WE} vs time for a Au(μ-WE) polarized at the fixed specified potentials recorded in deaerated 0.1 M $HClO_4$, (lower panel), while the Pt SE, placed at δ = 0.5 mm, was scanned between 1.2 and −0.25 and back to 1.2 V at a rate ν = 50 V/s (see magenta line in the upper panel), yielding the cyclic voltammogram (unfolded) in the upper panel (see blue line). **Insert**: Cyclic voltammogram of the Au(μ-WE) recorded at ν = 50 V/s in the same electrolyte showing the E_{WE} values selected for these measurements.

used as counter (CE) and reference electrodes (Ref-el), respectively. The SE was a Pt disk (Pine, AFE1B016PT, diameter 1.6 mm) placed directly above the WE aligned along its main axis (see Panel A, Fig. 1). Unless otherwise indicated, δ was set at ca. 0.5 mm. The potentials of the WE and SE were controlled independently using a Metrohm Autolab potentiostat/galvanostat (PGSTAT302 N) equipped with the BA module, which allows conventional rotating ring-disk measurements to be performed. The analogue output of the current to voltage converter of the Metrohm Autolab was digitized using an oscilloscope (Agilent, DSO-X 2014A) and stored for further processing. As specified above, E_{WE} was fixed at a prescribed value, while the potential of the SE, E_{SE}, was scanned at a fixed rate between two set limits. For these experiments, the cell was filled with ca. 35 mL of 0.1 M $HClO_4$ (OmniTrace Ultra), prepared with ultrapure water (UPW,18.3 MΩ, Barnstead water purifier) and placed in a Faraday cage to reduce noise and other electrical artifacts. Except where otherwise indicated, electrolytes were purged with Ar (Airgas, PP300) prior to the measurements.

3. Results and discussion

Two different model reactions were selected to illustrate the phenomenon of electrode stimulation: the formation of Au oxide on a Au(μ-WE) [14], and the oxidation of adsorbed carbon monoxide, CO_{ads}, on a Pt(μ-WE) [15] in aqueous acidic electrolytes. As reported in the cited references, both of these reactions have been found to follow Butler-Volmer type kinetics. The stimulation of the WE was effected by scanning the potential of the Pt SE disk between 1.2 and −0.25 V, a potential range in which the interfacial processes involved are of either capacitive, i.e. double layer charging and discharging, or pseudocapacitive, i.e. oxide formation and reduction, and hydrogen adsorption and desorption (*vide infra*), which allow the magnitude of the current to be modulated by controlling the scan rate.

3.1. Au oxide formation

The cyclic voltammogram of the Au(μ-WE) recorded at a scan rate ν = 50 V/s in deaerated 0.1 M $HClO_4$ (see insert, Fig. 3), displayed characteristic features ascribed to the formation of Au oxide for E > 1.0 V and its reduction for E < 0.9 V, during the scans in the positive and negative directions, E↑ and E↓, respectively. The potential of the Pt SE, E_{SE}, was set at 1.2 V for ca. 1 s, and then scanned at ν = 50 V/s down to −0.25 V, and back again to 1.2 V, yielding the "unfolded" voltammogram characteristic of this metal (see upper panel, Fig. 3). The current response of the Au(μ-WE), i_{WE}, during this scan for E_{WE} = 1.15 V, is shown in green in the lower panel,

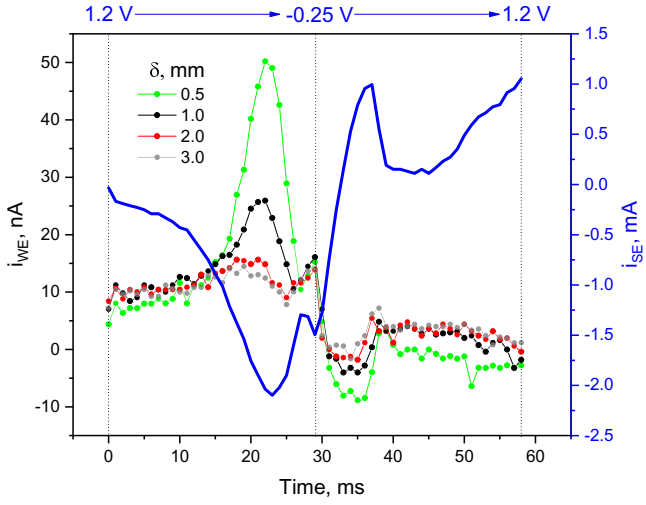

Fig. 4. Plots of i_{WE} as a function of time recorded under the same conditions as those specified in the caption Fig. 3, for E_{WE} = 1.15 V, for four different values of δ as specified. The blue line is the current flowing through the SE, i_{SE} (right ordinate).

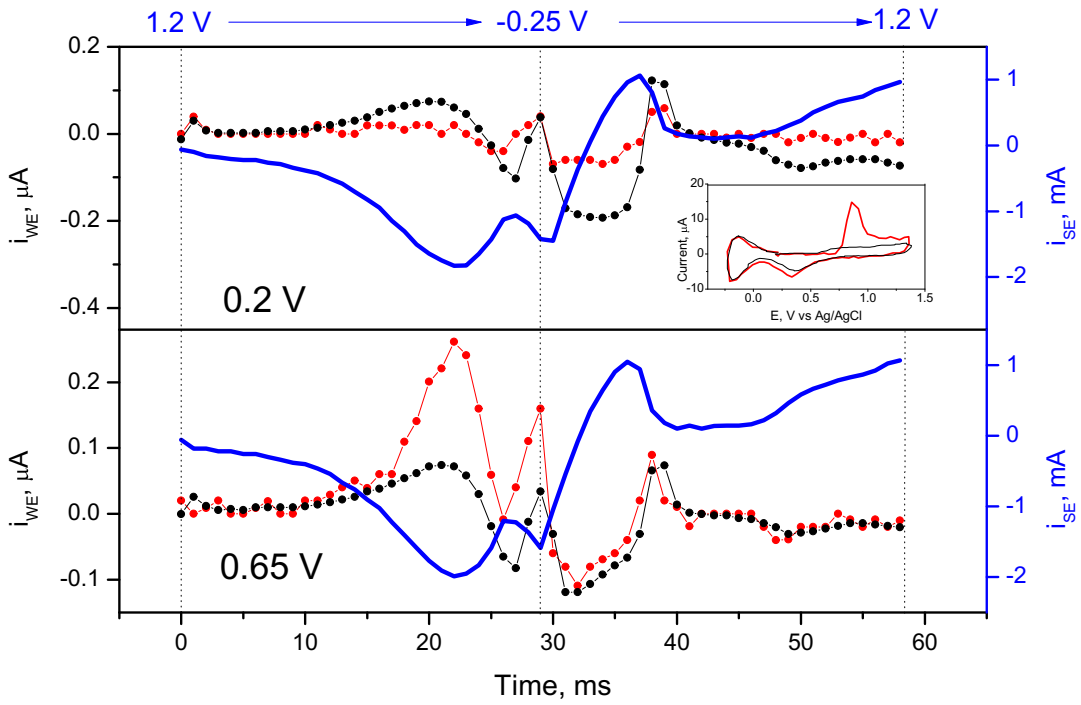

Fig. 5. Plots of i_{WE} vs time, recorded during the first cycle (see text for details) for a Pt(μ-WE) in deaerated 0.1 M $HClO_4$, while the Pt SE was scanned between 1.2 and −0.25 and back to 1.2 V at a rate $\nu = 50$ V/s (see blue line) for $E_{WE} = 0.2$ V (top panel) and 0.65 V (bottom panel) and $\delta = 0.5$ mm. The data in black and red symbols were obtained for the bare and CO_{ads} covered Pt(μ-WE), respectively. **Insert**: Cyclic voltammogram of the bare (black) and CO_{ads} covered (red) Pt (μ-WE) recorded at a rate $\nu = 50$ V/s in the same electrolyte.

Fig. 3. As clearly indicated, for $E_{SE} < 0.5$ V, during E↓, both $|i_{SE}|$ and $|i_{WE}|$ markedly increased, albeit in opposite directions, reaching a maximum at ca. 22 ms. Whereas $|i_{SE}|$ decreased by ca. 30% toward the end of E↓, $|i_{WE}|$ dropped to a very small value similar to that found prior to the stimulation. These results are consistent with the formation of Au oxide stimulated by a shift in η_s toward positive values induced by i_{SE} (see Fig. 1). In fact, the sudden drop in i_{WE} signals the end of Au oxide formation at the maximum applied η_s. During the entire E↑, i_{WE} was very small, indicating that η_s was not large enough to effect the reduction of the Au oxide formed. This is in agreement with the cyclic voltammogram of Au, for which the onset of Au oxide reduction is ca. 0.9 V (see insert, Fig. 3). Strong support for this explanation was provided by the very small and rather featureless i_{WE} response observed when the SE was initially scanned toward negative potentials for $E_{WE} = 0.4$ V (see black line, Fig. 3), i.e. in the middle of the double layer region of Au. For this smaller E_{WE}, the overpotential across the WE|electrolyte interface, induced by the passage of current through the SE, was insufficient to trigger Au oxide formation.

In contrast, hardly any changes in the i_{WE} response (except for a small increase in the negative current for $E_{WE} = 0.4$ V), were found during the subsequent scan of the SE toward positive potentials, both for $E_{WE} = 0.4$ V and 1.15 V, which suggests that the response is clearly unrelated to the reaction triggered by the SE during the initial scan toward negative potentials. Unfortunately, more work will be required to gain a better understanding of the shape of i_{WE} during this specific scan.

Strong evidence that the response of the WE is indeed derived from changes in ϕ_{dl} was provided by experiments in which the distance between the SE and WE, δ, was varied. As shown in Fig. 4, increasing δ led to a decrease in η_s, and, thus, a corresponding decrease in the magnitude of the peak current associated with Au oxide formation. This behavior, as well as the lack of proportionality between the peak current and δ, are both in agreement with theoretical predictions.

3.2. *The oxidation of CO_{ads} on Pt*

A second illustration of electrode stimulation was provided by analogue experiments involving the oxidation of CO_{ads} on a Pt(μ-WE). For these measurements, the CO_{ads} layer was assembled by bubbling CO (Airgas, 99.3%) into deaerated 0.1 M $HClO_4$ for ca. 10 min, followed by purging with Ar to eliminate solution-phase CO. Shown in the top panel, Fig. 5, are plots of i_{WE} vs time, for $E_{WE} = 0.2$ V, while scanning E_{SE} in the sequence 1.2

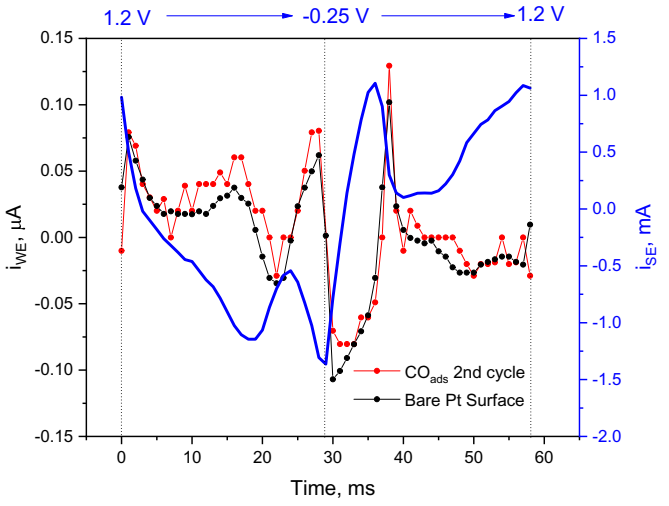

Fig. 6. Plot of i_{WE} vs time, recorded for a CO layer adsorbed on a Pt(μ-WE) polarized at $E_{WE} = 0.65$ V, during the second SE cycle (see text for details) in deaerated 0.1 M $HClO_4$ (see red line), while the Pt SE was scanned between 1.2 and −0.25 and back to 1.2 V at a rate $\nu = 50$ V/s (see blue line) at $\delta = 0.5$ mm. The corresponding data recorded for the bare Pt electrode under precisely the same conditions is shown in black line in this figure.

Table 1
Governing equations, boundary conditions and parameters employed in the simulations in dimensioned and dimensionless forms.

	Dimensioned	Dimensionless
Governing Equations	$\frac{\partial c_i}{\partial t} = -\nabla \cdot N_i, \quad i = H^+, \ ClO_4^-$	$\frac{\partial C_i}{\partial \tau} = -\tilde{\nabla} \cdot \tilde{N}_i$
	$N_i = -D_i \nabla c_i - D_i \frac{z_i F}{RT} c_i \nabla \Phi$	$\tilde{N}_i = -\tilde{D}_i \tilde{\nabla} C_i - Z_i C_i \tilde{\nabla} \Phi$
	$\nabla^2 \Phi = \frac{F}{\varepsilon_0 \varepsilon_r} \sum z_i c_i$	$\tilde{\nabla}^2 \tilde{\Phi} = \frac{1}{\tilde{\varepsilon}} \sum Z_i C_i$
Boundary Conditions	$-N_{H^+}\big\|_{y=0, r<r_e} = c_{H^+} k_f - k_b$	$-\tilde{N}_{H^+}\Big\|_{Y=0, R<1} = (C_{H^+} K_F - K_B)$
	$k_f = k_{bv} e^{(1-\beta) nF(E-\Phi)/RT}$	$K_F = K_{BV} e^{(1-\beta) n(V-\tilde{\Phi})}$
	$k_b = k_{bv} e^{(-\beta) nF(E-\Phi)/RT}$	$K_B = K_{BV} e^{(-\beta) n(V-\tilde{\Phi})}$
	$i = F \int_0^{r_e} N_{H^+}\big\|_{y=0} 2\pi r dr$	$i = F D_{H^+} c_1^{\infty} r_e \int_0^1 \tilde{N}_{H^+}\Big\|_{Y=0} 2\pi R dR$
Variables and Parameters	$C_i = c_i / c_{H^+}^{\infty}, \quad \tilde{D}_i = D_i / D_{H^+}, \quad Y = y/r_e, \quad R = r/r_e$	
	$V = E(F/RT), \quad \tilde{N}_i = \frac{r_e}{D_{H^+} c_{H^+}^{\infty}} N_i, \quad K_{BV} = r_e k_{bv} / D_{H^+} = \tilde{\Phi}(F/RT), \quad \tilde{\varepsilon} = \frac{\varepsilon_0 \varepsilon_r RT}{a_{np}^2 F^2 c_{H^+}^{\infty}}$	

$\rightarrow -0.25 \rightarrow 1.2$ V at $\nu = 50$ V/s both for the bare (black curve) and CO covered Pt(μ-WE) (red curve). As indicated in the insert, this potential is well within the double layer region of Pt in this electrolyte, and far negative to the onset of CO_{ads} oxidation. The differences in i_{WE} are due to the decrease in the interfacial capacity induced by adsorption of CO [16–18]. Also shown in blue in this panel is a plot of i_{SE} vs time (unfolded CV). In stark contrast to the results shown in the top panel, Fig. 5, a large i_{WE} peak was found for $E_{WE} = 0.65$ V (see red curve in the bottom panel, Fig. 5), while E_{SE} was scanned from 1.2 V toward negative potentials, a region in which i_{SE} is associated with the reduction of Pt oxide (see blue curve). According to the cyclic voltammogram, $E_{WE} = 0.65$ V is very close to the onset of CO_{ads} oxidation (see insert in this figure). In analogy to the phenomenon described in the previous section, we ascribe this behavior to an increase in η_s induced by the negative i_{SE}, which will promote oxidation of CO_{ads}. Further evidence in support of this explanation was provided by the disappearance of the peak during the subsequent cycle, which yielded a response virtually identical to that of a bare Pt(μ-WE) (see Fig. 6). The much larger i_{WE} observed for $E_{WE} = 0.20$ V compared to 0.65 V during the scan of the SE toward positive potentials is most likely related to the adsorption of hydrogen on Pt.

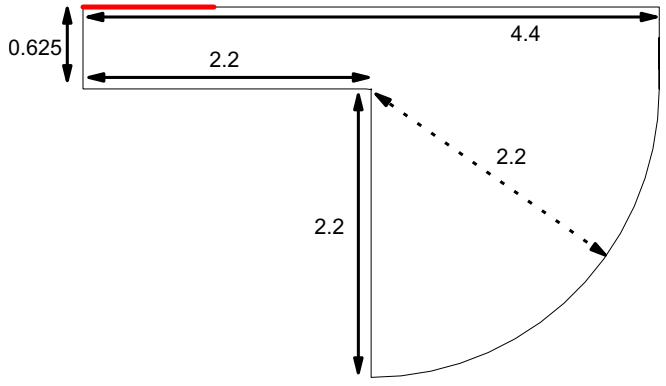

Fig. 7. Schematic diagram of the domain employed in our simulations where the numbers refer to dimensionless distances. The red segment represents the stimulating electrode, whereas all other boundaries are insulating, except the round boundary up to the horizontal edge, for which the electrostatic potential was set at zero. Not included in this domain is the segment that would represent the working electrode as this is not of concern in the simulations pursued in this work.

3.3. Theoretical simulations

The primary aim of this section is to assess whether the composition of the electrolyte in the region neighboring the working electrode, WE, would be affected by the passage of current through the stimulating electrode, SE, under conditions which closely mimic those employed in the actual experiments. This issue is of concern, as the local concentration of solvated protons, $H^+(aq)$ would alter the rate of the reactions selected for this study. Specifically, reduction reactions at the SE, in this case, i.e.

$$PtO_2 + 4\,H^+(aq) + 4e^- \rightarrow Pt + 2H_2O \text{ and}$$
$$H^+(aq) + e^- \rightarrow PtH \qquad (2)$$

will lower the proton concentration in its immediate vicinity, an effect that will propagate to the WE and thus increase the rate of its oxidation. To this end, COMSOL was used to solve the coupled material-balance equations for each of the species involved, i.e.

$$\frac{\partial c_i}{\partial t} = D_i \nabla^2 c_i + z_i F u_i \nabla \cdot (c_i \nabla \Phi) \qquad (3)$$

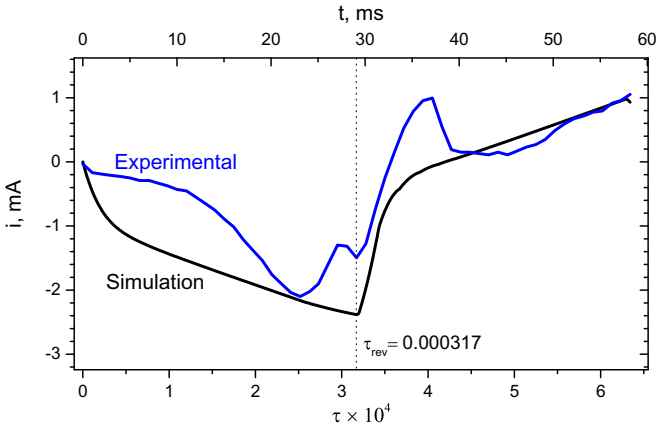

Fig. 8. Plots of the experimental (blue) and simulated (black) currents flowing through the SE, as a function of the dimensionless (lower abscissa) and dimensioned (upper abscissa) time.

where c_i is the concentration, D_i, z_i, and u_i are the diffusion coefficient, number charge and mobility of species i, i.e. solvated H^+, and ClO_4^-, in our case, and Φ is the electrostatic potential in solution, where the latter satisfies Poisson's equation, i.e.

$$\nabla^2\Phi = \frac{F}{\epsilon_0\epsilon_r}\sum z_i c_i \tag{4}$$

subject to the boundary conditions in Table 1. As specified therein, the electrochemical reactions associated with the passage of current through the SE were assumed to follow Butler-Volmer kinetics, where the reduction process (oxide reduction) was assumed to be of first order in solvated protons, and the reverse reaction (oxide formation), which generates solvated protons, of zeroth order in the same species. Accordingly, the negative and positive currents flowing through the SE can be correlated to the number of protons consumed or generated during oxide reduction and formation, respectively.

The program implementation was validated using a model reported by Baker and Verbrugge in their studies of copper deposition on a microdisk electrode embedded in an insulating surface [19]. For those calculations, selection of a judicious domain and mesh yielded values for all the variables involved within 2% of those reported by these authors. The axisymmetric domain used to represent the cell|electrode arrangement used in our experiments is shown in Fig. 7, where the red line represents the SE, where the numbers represent dimensionless distances based on the actual dimensions of the SE and associated insulating shroud, and of an insulating solid cylinder placed parallel to the SE at the same dimensional distance as the WE in the actual experiments, including its own insulating shroud. Kinetic parameters were selected so as to approximate the current response to a potential scan applied to the SE. The plots of the actual current flowing through the SE (blue trace) and that generated from the simulation (black trace), assuming $K_{BV} = 1$ and $\beta = 0.5$ (see Table 1) are given in Fig. 8. Since the main goal of the simulations is to assess the changes in solution composition in the region adjacent to the WE (*vide supra*), the differences between the simulated and actual currents, as well as the absence of the WE, should not be of concern. Shown in Fig. 9 is a concentration map representing the

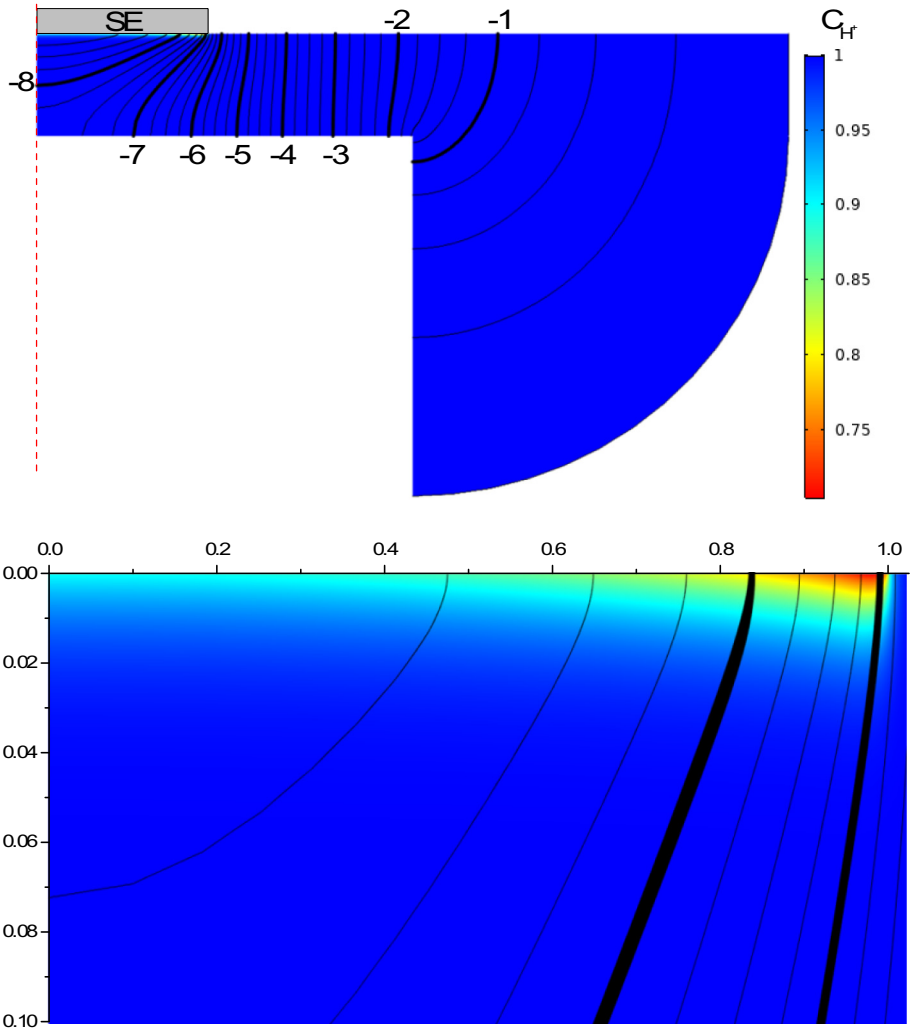

Fig. 9. Top Panel. Concentration map of C_{H^+} in the domain selected for the simulations which approximates that employed in the actual experiments, at $\tau_{rev} = 0.000317$, i.e. the actual time at which the potential scan applied to the SE was reversed. The lines represent equally spaced equipotentials for the values specified around the domain in intervals of 0.25 dimensionless units. **Bottom Panel**. Expanded section of the concentration map in the Top Panel in this figure in the vicinity of the SE, where the vertical scale was stretched by a factor of 10 for clarity. Note that the horizontal and vertical axes in this panel represent dimensionless distances along the surface, and normal to the center of the stimulating electrode, respectively.

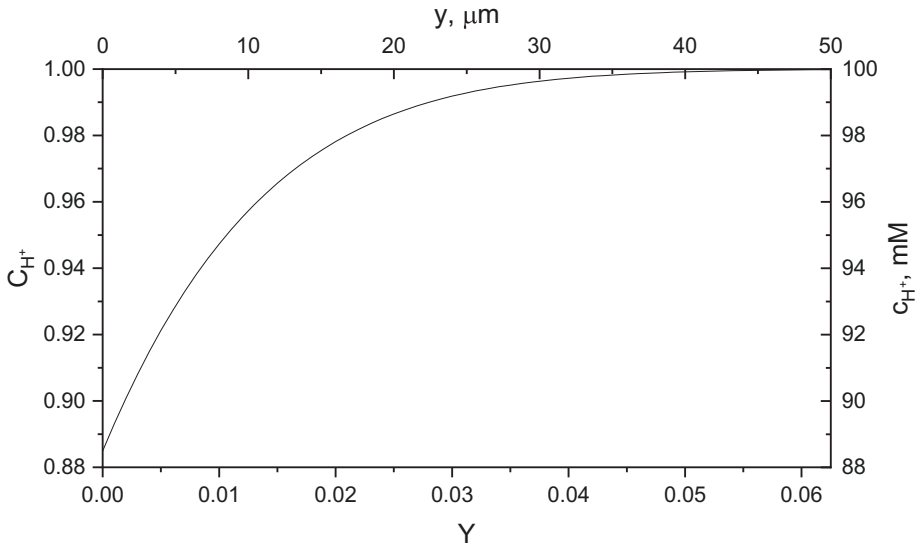

Fig. 10. Plot of C_{H^+} (left axis) and c_{H^+} as a function of Y (bottom axis) and y (top axis) at $\tau_{rev} = 0.000317$, i.e. 29 ms, the time at which the linear scan was reversed (see Fig. 8).

dimensionless concentration of solvated protons, C_{H^+}, at a dimensionless time, $\tau_{rev} = 3.17 \times 10^{-4}$, which corresponds to the actual time at which the potential scan applied to the SE was reversed, $t_{rev} = 29$ ms. The lines in this figure are the corresponding equipotentials for the values specified around the domain in intervals of 0.25 dimensionless potential units. An expanded view of this figure in the vicinity of the SE is depicted in the Lower Panel in this figure, where the vertical scale was stretched by a factor of 10 for clarity. A better illustration of the changes in C_{H^+} induced by the passage of current through the SE is given in Fig. 10, which displays a plot of C_{H^+} along the center line normal to the SE surface, which coincides with the corresponding normal to the surface of the WE, at $\tau_{rev} = 3.17 \times 10^{-4}$. As indicated therein, C_{H^+} at the surface of the SE was ca. 0.885, and increased to reach virtually unity, i.e. bulk concentration, at Y = 0.6, i.e. 48 μm. This distance is about an order of magnitude smaller than the smallest separation between the SE and WE used in our experiments, i.e. d = 500 μm. Virtually identical results were obtained by enlarging the domain in Fig. 7, keeping the dimensions of the two electrodes, as well as the magnitudes of all other parameters the same. On this basis, any current flowing through the WE may be ascribed solely to changes in the electrostatic potential in its immediate vicinity induced by passing current through the SE.

4. Conclusions

As clearly demonstrated by the illustrations provided, the method herein described makes it possible to change the electrostatic potential in the neighborhood of an electrode polarized at a fixed potential with respect to a conventional reference electrode, and, thus, enhance the rates of a redox reaction involving adsorbed species. Particularly exciting are the prospects of inducing highly localized reactions involving adsorbed species and monitor the dynamics of surface processes, such as diffusion and reaction propagation, using a variety of optical techniques. Such experiments are currently in progress and will be reported in due course.

Declaration of competing interest

None.

Acknowledgements

This work was supported by a grant from NSF, CHE-1808592.

References

[1] J.S. Newman, K.E. Thomas-Alyea, Electrochemical Systems, third ed., J. Wiley, Hoboken, N.J, 2004.
[2] A.J. Bard, L.R. Faulkner, Electrochemical Methods: Fundamentals and Applications, second ed., Wiley, New York, 2001.
[3] J. Newman, Resistance for flow of current to a disk, J. Electrochem. Soc. 113 (1966) 501–502.
[4] T.M. Braun, D.T. Schwartz, Localized electrodeposition and patterning using bipolar electrochemistry, J. Electrochem. Soc. 162 (2015) D180–D185.
[5] S.E. Fosdick, K.N. Knust, K. Scida, R.M. Crooks, Bipolar electrochemistry, Angew. Chem. Int. Ed. 52 (2013) 10438–10456.
[6] Y.U. Kayran, V. Essmann, S. Grutzke, W. Schuhmann, Selection of highly SERS-active nanostructures from a size gradient of Au nanovoids on a single bipolar electrode, Chemelectrochem 3 (2016) 399–403.
[7] Y. Chen, A. Belianinov, D. Scherson, Spatially-resolved interfacial electrochemistry: ohmic microscopy, J. Phys. Chem. C 112 (2008) 8754–8758.
[8] C.A. Cartier, D. Kumsa, Z. Feng, H. Zhu, D.A. Scherson, Quantitative aspects of ohmic microscopy, Anal. Chem. 84 (2012) 7080–7084.
[9] Z. Feng, N.S. Georgescu, D.A. Scherson, New advances in ohmic microscopy, Russ. J. Electrochem. 53 (2017) 1003–1010.
[10] S.F. Cogan, Neural stimulation and recording electrodes, Annu. Rev. Biomed. Eng. 10 (2008) 275–309.
[11] C. Gabrielli, H. Takenouti, M. Keddam, Study on distribution of potential on surface of ring-disk electrode, J. Chim. Phys.-Chim. Biol. 69 (1972) 707–&.
[12] J.J. Miksis, J. Newman, Primary resistances for ring-disk electrodes, J. Electrochem. Soc. 123 (1976) 1030–1036.
[13] D. Trinh, E. Maisonhaute, V. Vivier, Electrical cross-talk in transient mode of scanning electrochemical microscopy, Electrochem. Commun. 16 (2012) 49–52.
[14] J.W. Schultze, K.J. Vetter, Kinetics of electrochemical formation and reduction of monomoleculat oxide films on gold, Berichte Der Bunsen-Gesellschaft Fur Physikalische Chemie 75 (1971) 470–481.
[15] P. Inkaew, C. Korzeniewski, Kinetic studies of adsorbed CO electrochemical oxidation on Pt(335) at full and sub-saturation coverages, Phys. Chem. Chem. Phys. 10 (2008) 3655–3661.
[16] J.M. Feliu, J.M. Orts, R. Gomez, A. Aldaz, J. Clavilier, New information on the unusual adsorption states of Pt(111) in sulfuric acid solutions from potentiostatic adsorbate replacement by CO, J. Electroanal. Chem. 372 (1994) 265–268.
[17] K. Domke, E. Herrero, A. Rodes, J.M. Feliu, Determination of the potentials of zero total charge of Pt(100) stepped surfaces in the [011] zone. Effect of the step density and anion adsorption, J. Electroanal. Chem. 552 (2003) 115–128.
[18] A.J. Bard, C. Zoski, Electroanalytical Chemistry : a Series of Advances, CRC Press, Hoboken, 2011, 2011.
[19] M.W. Verbrugge, D.R. Baker, Transient diffusion and migration to a disk electrode, J. Phys. Chem. 96 (1992) 4572–4580.